



Geological setup and physicochemical characteristics of Munger Groups of thermal springs along Munger–Saharsa Ridge Fault, Bihar, India: A conceptual hydrogeochemical model

ARCHISMAN DUTTA^{1,2,*} , AYODHAYA PRASAD THAPLIYAL¹, PRAMOD KUMAR SINGH¹, SANDEEP ROHILLA¹ and RAMESH KUMAR GUPTA¹

¹Geological Survey of India, Northern Region, Lucknow 226 024, India.

²Department of Chemistry, Institute of Science, Banaras Hindu University, Varanasi, India.

*Corresponding author. e-mail: duttaarchisman1@gmail.com

MS received 10 March 2022; revised 27 July 2022; accepted 28 August 2022

The hydrogeochemistry of hot springs located along the vast stretch of Munger–Saharsa Ridge Fault (MSR) zone in the Rajgir–Munger metasedimentary belt of eastern peninsular India is investigated. The temperature of springs lies between 25° and 65°C, with the highest surface manifestation in Bhimband. The thermal springs are issued from joints and fractures along MSR, East/West Patna faults of Precambrian quartzites and phyllites. The major ion composition elucidates that majority of waters are Ca–Mg–HCO₃ type. The mechanisms controlling rock dominance origin of cations and both precipitation and rock dominance origin of anions in thermal waters are silicate rock weathering and ion-exchange processes between aquifer-rock and water. The mixing models illustrate that cold water causes intense dilution of geothermal fluids before discharge, with highest contribution in Bhaduria Bhar (76.6%) and lowest in Bhimband (55.4%) springs. The reservoir temperature as estimated based on quartz geothermometry ranges ~100°C grading springs as low enthalpic geothermal resources. Near-surface dilution disturbs Na/K-geochemical equilibrium and thus multi-component geothermometry furnish inaccurate results. Mineral phase saturation studies depict near equilibration of quartz and chalcedony with thermal waters. With all evidences of hydrogeochemical modelling, a conceptual model of recharge-mixing-discharge of thermal springs is proposed in the study.

Keywords. Munger–Saharsa Ridge (MSR) Fault; tectonics; hydrogeochemistry; mixing models; geothermometry; geothermal gases.

1. Introduction

There has been an increase in interest in recent years in investigating alternative energy resources that are comparatively cleaner and more sustainable than fossil fuels. One such pure, largely

pollution-free, enduring, and sustainable alternative energy source is geothermal energy. The surface signatures of these geothermal sources are manifested through hot springs, natural geysers, fumaroles, etc. (Kresic 2010; Chatterjee *et al.* 2022; Goswami *et al.* 2022). Regions with heat

flow value greater than global average of 63 mW/m² are identified as geothermal provinces (Chandrasekharam and Bundschuh 2008). The Ministry of New and Renewable Energy (MNRE), Government of India, is envisioned to launch geothermal energy plants with a harnessing capacity of 1000 MW by 2022 (Sarolkar 2018). Hydrothermal manifestations can be exploited for balneotherapy, geo-tourism, aquaculture, greenhouse cultivation, etc., apart from power generation (Shanker 1991; Sarolkar 2018). The Indian geothermal springs bear various religious beliefs and myths of contemporary Indian culture and Rajgir in Bihar, Tuwa in Gujarat, Gangotri, Yamunotri, Kedarnath and Badrinath (Chardham) in Uttarakhand, etc., are worth mentionable as from ancient times, thermal springs are considered to possess divine strength of God (Mehta and Chowdhary 1966). Geological Survey of India has divided Indian geothermal systems into two broad domiciles based on enthalpy manifestation of thermal springs: medium enthalpy and low enthalpy geothermal provinces with surface temperature manifestation of 75°–100°C and 35°–75°C, respectively (Dutta *et al.* 1982; Krishnaswamy and Shankar 1982; GSI 1987, 1989, 1991, 2016). The medium enthalpy geothermal provinces comprise younger intrusive granites with highly sheared zones, thrust faults, strike, etc., in Puga–Chumathang, Parbati, Beas, and Satluj Valley, where regional heat flow is above 180 mW/km² (Shanker 1991). The medium to low enthalpy geothermal province lies across major tectonic features/lineaments, slip-faults and faults in Son–Narmada–Tapti or SONATA lineament zone across Salbardi, Tapti, Rajgir–Munger in Bihar, Tatta and Jarom in Jharkhand, Satpura areas of Maharashtra with regional heat flow of 100–180 mW/km² and Eastern Ghats of Orissa, grabens, and rifts of Gondwana basins of Damodar Valley, Godavari and Mahanadi basin, and Quaternary sediments across the Cambay basin of West Coast with heat flow of 70–100 mW/km² (Shanker 1991; Valdiya 2015). The low enthalpy geothermal manifestation is associated with neotectonism and tertiary tectonic activities and is found in the Siang Valley of Arunachal Pradesh (Chatterjee *et al.* 2022; Dutta and Gupta 2022).

The Rajgir–Munger metasedimentary springs fall under the classification of geothermal system called continental rift geothermal system that does not possess any active volcanic activities at

the present date with meagre tectonism (Shanker 1991; Chandrasekharam and Bundschuh 2008). The Munger–Rajgir metasedimentary belt of Bihar, India is associated with Miocene to Pleistocene faults of late-phase Himalayan orogeny occurring isoclinal across folded quartzites with interbedded and cross-bedded phyllites, near peninsular India (Sarkar and Basu Mallick 1982; Roy *et al.* 1987; Singh *et al.* 2015a, b). Bhagwan Das (1967) and Mazumdar (1988) linked the Munger–Rajgir Formation to sub-metamorphic rocks in central India's Son and Narmada valleys, suggesting that the Munger–Rajgir Formation might be an orogenic unit. By K–Ar dating, Sarkar *et al.* (1964) determined the age of quartzite from the eastern half of the Munger–Rajgir area to be 358–420 million years. There are 24 hot springs in the location, which are studied with a temperature of thermal waters varying from 26° to 65°C and are classified into two major groups, i.e., Rajgir Group and Munger Group of hot springs (Razdan *et al.* 2008; Gautam *et al.* 2018a, b). The Rajgir Group consists of Rajgir, Tapoban, and Agnikund hot springs, whereas the Munger Group consists of Rishikund–Bhurkha, Sitakund, and Bhimband hot springs. The majority of thermal springs in the Munger–Rajgir metasedimentary belt are found along the MSR fault zone, interbedded with shale bands of quartzite and phyllite, where the crushed rocks of the fault zone may act as a barrier for forcing hot water out on the surface as geothermal manifestation. The Munger–Rajgir metasediments, on the other hand, have been represented as probably time comparable with the lower Vindhyan in the most recent geological map of India released by the Geological Survey of India (1998). These have undergone little metamorphism (Sarkar and Basu Mallick 1982), and their general lithology and structure differ from the Vindhyan series. These hot springs emanate from both hill slopes and river beds. In due course of large-scale geological mapping (LSM) of 25 km² on a 1:12500 scale, noticeable faults, fault zone, fault breccia, highly silicified zones, and prominent lineaments were delineated and mapped, wherever feasible (GSI 2021). Geological control of hot springs has been identified in the studied area and most of the springs are located near noticeable faults of considerable length. The faults have been traced and signatures of faulting are recorded. Most of the geothermal hot springs do not contain

geothermal deposits and have a feeble sulfurous smell. The recent works by Singh *et al.* (2015a, b) in Rajgir–Munger metasedimentary springs put forth the gravity anomaly geophysical data where negative anomaly (–50 mGal) value suggests presence of granites as the heat providing source of circulating fluids like the Bakreshwar–Tantloi areas. The Munger–Saharsa Ridge Fault zone, which is an extension of SONATA lineament, exhibit multiple thermal manifestation with comparatively slow discharge rates than Tattapani geothermal system, where sedimentary insulation is provided to intrusive granites even up to 2 km depth, thus producing a high geothermal gradient ($>50^{\circ}\text{C}/\text{km}$) (Pandey 1975; Chandrasekharam and Prasad 1998; Chandrasekharam *et al.* 2006).

In the present study, an attempt has been made to study the interrelationship between the geothermal manifestations with the geo-tectonic features of the study area in correlation with various possible aspects responsible for chemical variations in thermal discharges. Major ion concentrations are assessed to illustrate the hydro-geochemical evolution of the thermal springs in the study area. Various 2D scatter plots are done to comprehend geochemical origin of thermal waters. Mineral saturation indices are computed to elucidate the state of dissolution of various minerals in thermal waters. The extent of mixing of thermal water with cold spring waters is estimated and based on which the reservoir temperature is estimated using both chemical geothermometers and multi-component geothermometers as determination of subsurface temperature is essential from a utilitarian perspective. In this study, efforts are made to collect and analyse the gas samples emanating from multiple gas outlets over the surface of geothermal springs to get clear insights about a possible source of heat generation of thermal springs, based on which a conceptual model has been illustrated. In a nutshell, targets of the present study are: (i) to rationalise the geochemical evolution of solutes in thermal water, (ii) variation of various mineral concentrations with the variation of temperature, (iii) evaluation of geothermal gases, (iv) determining the extent of mixing of hot spring waters with non-thermal waters, (v) calculation of the reservoir temperature using both chemical and multi-component geothermometers, and (vi) to build a conceptual hydrogeochemical model demonstrating the recharge source to

groundwater circulation and finally to emanation as hot springs of the study area.

2. Geological setup of the study area

2.1 *Geology and regional structural setting*

The study area lies in parts of Munger, Nalanda, Nawada, Lakhisarai, and Gaya districts of Bihar. It forms a part of the Munger–Rajgir Group, occurring as inselbergs within vast stretches of alluvium all around, and it is located in the northern domain of Chhotanagpur Gneissic Complex. Location-wise, the Chhotanagpur Granite–Gneiss Complex (CGGC) is circumscribed by Gangetic alluvium plains in the north, Singbhum mobile belt, and Rajmahal basalt in the south and northeast, respectively. The northern side of CGGC lies the Munger–Saharsa Ridge (MSR) Fault zone which is associated with Kharagpur hills and is the location of the majority of thermal springs of Munger (Sarkar and Basu Mallick 1982; Chatterjee and Ghose 2011) (figure 1a). The area falls in Survey of India, toposheet nos. 72G/08, 72H/05, 72K/11, 72K/08, 72K/04, and 72K/12 and bounded within latitudes 24.5:25.5N: longitudes 85.0:86.75E.

From a geomorphological perspective, the study area is exposed with several trend lines of varying structural manifestations like faults, intense folds, lineaments, etc., along the Kharagpur hills which lithologically consist of quartzite, phyllite, schist, and slate of Precambrian age (Roy *et al.* 1987). Regionally, the Munger–Rajgir metasedimentary belt encompasses the ENE–WSW trending Rajgir fold belt with elongated hill range and consists of alternate quartzite and phyllite bands of Mesoproterozoic age. Rai and Dayal (1971) mentioned about quartzite, phyllite, schist, and gneisses lying across E–W or ENE–WSW strike, while the eastern side of the Kharagpur hills consists of the major fault along N–S direction. Several faults have displaced the quartzite bands and a few longitudinal and shear faults have also been recognised. The thermal springs of Munger occur in the eastern domain of the Kharagpur hill range of the Rajgir–Munger fold belt.

2.2 *Seismotectonics of the study area*

All the thermal springs ooze out from isoclinal folds of meta-sedimentary Kharagpur hill range along

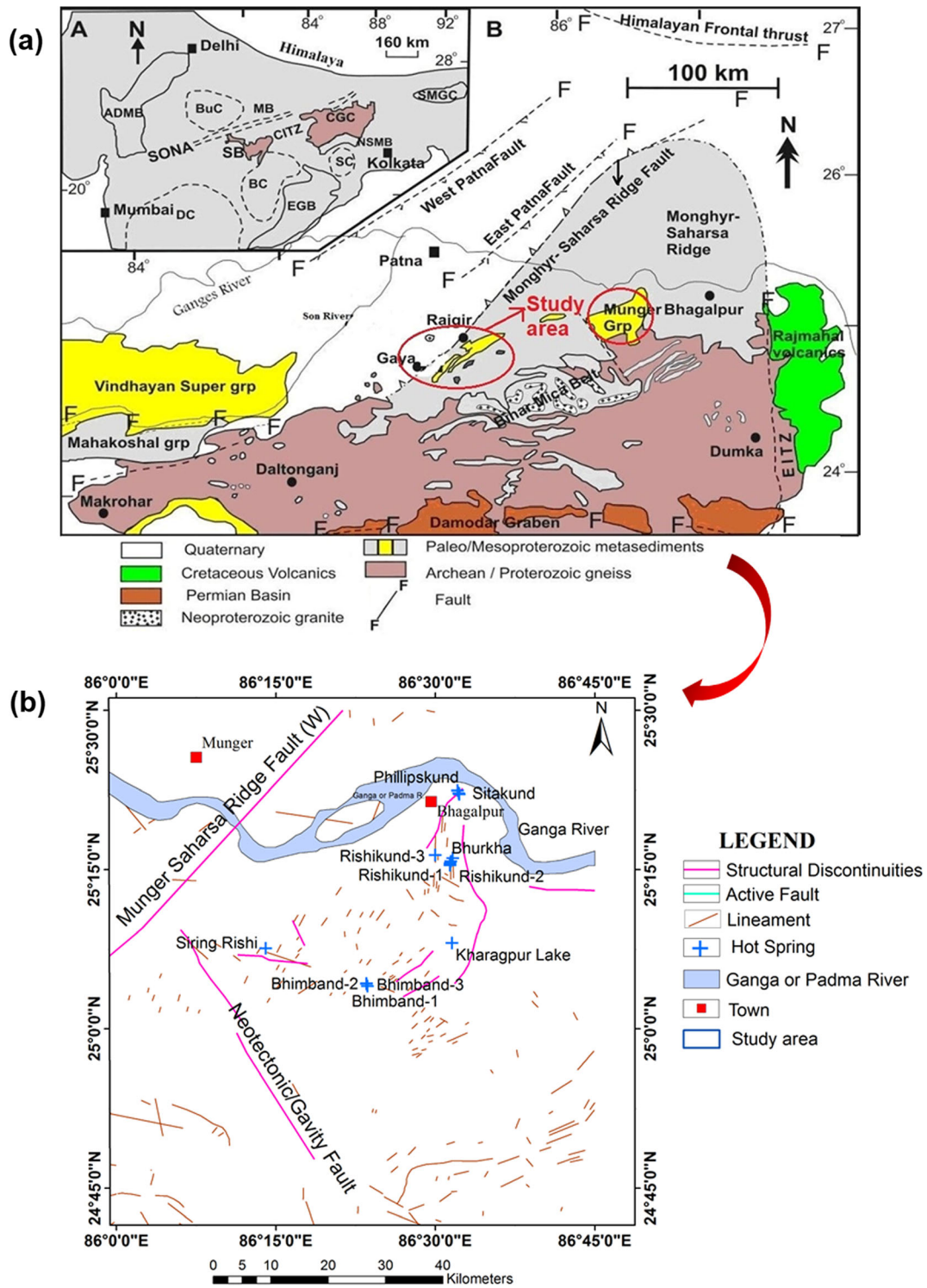


Figure 1. (a) Regional geological map of the area with various structural manifestations (modified after Chatterjee and Ghose 2011) and (b) geotectonic lineament map showing structural features and hot spring locations.

MSR fault zone except Sitakund group of thermal springs, which issue along Gangetic alluvium. The area is traversed by quite old faults; neo-tectonic activity along these faults is not recognisable. Major earthquakes are, however, recorded in the

past from Munger and adjacent areas. Two trends of lineaments comprising of enechelon faults are observed in Munger, where the first group of lineament occurs in the Kharagpur hill area of late Proterozoic time, truncated through N-S in the

eastern part of NW–SE in the western part. The second group of lineaments has two components: one, along E–W trending faults in the course of Ganga, and another one, ENE–WSW trending fault along the margin of Chhotanagpur upland. The two groups of lineaments merge at Sitakund hot spring and continue eastward along Ganga up to Rajmahal hills delineating up to southern limit of Ganga trough and further affecting Kharagpur hills. The Bhimband hot spring is located on the southern part of the Kharagpur hill, along the intersection of fault zone trending ENE–WSW and NNE–WSW. The metasedimentaries have a steep dip of 70–80° and strike changing from ENE–WSW in the west to NNE–SSW in east and N–S in the north. The other hot springs monitored are Rishikund-1, 2, 3, and 4, Bhurkha, and Bhaduria Bhar, Kharagpur Lake, and Siringrishi (figure 1b of ESI).

3. Data and methodology

Fourteen hot springs and two cold spring water samples are collected in air-tight high-density polypropylene bottles from various areas of the Munger and Lakhisarai districts of Bihar from January to February 2021. Water samples are preserved by adding concentrated HNO₃ (Merck Suprapure) for laboratory analysis of trace and rare earth elements by inductively coupled plasma mass spectrometer (VARIAN 820 MS). The physical parameters (pH, electrical conductivity) are measured by using Systronics μ pH system 361, Systronics conductivity meter with cell constant 1.0 ± 10%, respectively and the major ions (Ca²⁺, Mg²⁺, Na⁺, K⁺, SO₄²⁻, NO₃⁻, HCO₃⁻, F⁻, Cl⁻, SiO₂, PO₄³⁻) are analysed using standard operating procedures. Amongst the major ions, Ca²⁺, Mg²⁺, HCO₃⁻, and Cl⁻ are analysed by using the standard titrimetric method (APHA 1985). Amongst the other ions, Na⁺ and K⁺ are analysed using Systronics 128 Flame Photometer; SO₄²⁻, NO₃⁻, SiO₂, and PO₄³⁻ are analysed using Thermo (UV330) UV spectrophotometer, and F⁻ is estimated using Thermo Scientific Ion-Selective Electrode (ISE). The precision of the chemical analysis is justified by normalised inorganic charge balance, which lies within ±5%.

The distributions of main ion concentrations were utilised to create a Piper trilinear diagram, which was then used to understand the thermal water quality in distinct geothermal provinces. The Piper diagram in GW Chart 1.30.0 software.

Other hydrogeochemical parameters like Giggenbach triangular diagrams (Na–K–Mg and Cl–SO₄–HCO₃) are plotted using Liquid Analysis v1 Powell-2010-StanfordGW excel spreadsheets (Powell and Cumming 2010).

Six gas samples are collected from gases emanating from the hot springs of Munger. The gas samples are collected in Tedlar gas sampling bags, each of volume 1000 cm³ and proper precautionary measures are adopted while collecting gas samples to avoid any kind of areal gas contamination. The sampling of gases has been primarily done during the winter season in January–February, 2021. The collected gas samples are analysed in VARIAN 450 GC Gas Chromatograph equipped with thermal conductivity detector (TCD) in Chemical Laboratory, Geological Survey of India, Lucknow, and the instrument is calibrated by internationally accepted gas standards of permanent gas and real gas. The high-purity zero air, helium, and nitrogen gases are used as carrier gases in the experiments.

3.1 Geochemical and geothermometry

Geothermometers are used to estimate sub-surface reservoir temperature based on the chemical composition of the thermal spring water. Based on mineral solubility and exchange reactions of ions, geothermometers are divided into two categories: quartz geothermometry (reservoir temperature dependent on the concentration of quartz as reactive species) and cation geothermometry (exchange reactions between Na–K; K–Mg, etc.). It can be fundamentally stated that relative abundance of a particular mineral/or dissolved species, which plays a dominant role in rock–water interaction, thus governing geochemical equilibrium, prioritise its use as a geothermometer to estimate reservoir temperature (Fournier 1977; Arnórsson *et al.* 1983). However, for accurate estimation of reservoir temperature, fast ascending geothermal fluids with high chloride concentration are ideal as they retain deep-seated reservoir information, have higher residence period, and have a minimum chance of mixing with cold water, steam loss, dilution, etc. The mixing of shallow groundwater might alter the equilibration conditions, causing uncertainty in reservoir temperature estimation. The quartz geothermometry is based on the solubility of silica minerals with temperature which increases maximum up to 250°C, beyond which quartz solubility decreases and geothermometry

fails to predict accurate reservoir temperature (Fournier and Truesdell 1974). The important geothermometers used to calculate the reservoir temperatures are listed below:

Quartz geothermometer with no steam loss (adiabatic):

$$T (^{\circ}\text{C}) = (1309/5.19 - \log S) - 273.15$$

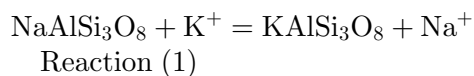
Quartz geothermometer with maximum steam loss (conductive):

$$T (^{\circ}\text{C}) = (1522/5.75 - \log S) - 273.15$$

where $S = \text{SiO}_2$ concentration is in mg/l.

The multi-component geothermometry is also used to determine reservoir temperatures based on attainment of equilibrium conditions of water through water–rock interactions and long residence time between wall rock and geothermal waters (Goswami *et al.* 2022). However, partially or fully equilibrated waters are suitable for this geothermometry over immature waters as per Na–K–Mg diagram. Giggenbach (1988) combined the two different ion-exchange reactions: (i) ion exchange between Na–K, which occurs at high temperature at a slow rate and in greater reservoir depth, and the other one (ii) K–Mg reaction, which occurs rapidly at relatively lower temperature and at shallow depth, into a single ternary plot to indicate the suitability of thermal waters for reservoir temperature estimation. Waters are categorised into three major domains: fully equilibrated water, partially equilibrated water, and immature water (Giggenbach 1988). The applicability of the diagram lies in predicting the reservoir temperature by ascertaining the fluid concentration of the latest equilibrium. The important geothermometers used to calculate the reservoir temperatures in this context is manifested by:

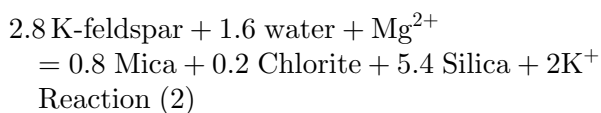
For geochemical temperature-dependent equilibrium exchange reactions:



$$K_{\text{eq}} = [\text{Na}^+]/[\text{K}^+]$$

The geothermometry equation follows:

$$T (^{\circ}\text{C}) = 1390/1.75 + \log([\text{Na}^+]/[\text{K}^+]) - 273.15$$



$$K_{\text{eq}} = [\text{K}^+]^2/[\text{Mg}^{2+}]$$

The geothermometry equation follows:

$$T (^{\circ}\text{C}) = 4410/14.0 + \log([\text{K}^+]^2/[\text{Mg}^{2+}]) - 273.15.$$

3.2 Mineral saturation indices

The mineral saturation indices are computed using PHREEQC software package using the *wateq4f* thermodynamic database (Parkhurst and Appelo 1999). The saturation index (SI) can be defined as the logarithmic ratio of ion activity product and solubility of a mineral at a particular temperature and pressure. The value of SI indicates the extent of saturation of water with a particular mineral phase with positive value indicating supersaturation and precipitation of a mineral in water, negative value indicating undersaturation and dissolution of that mineral in water and zero value indicates the equilibrium condition where both precipitation and dissolution of that mineral are occurring at same rate. Hence, it can be said that the temperature at which SI value is ~ 0 and mineral assemblages tend to converge, equilibrium condition prevails in the reservoir at that temperature with that mineral and the said temperature will be the reservoir temperature (Tole *et al.* 1993).

In the SI calculations, common lithotypes are always followed mainly: siliceous minerals are represented by quartz, amorphous silica and chalcedony; clastic and igneous rock minerals are represented by feldspar, albite and anorthite; clay minerals are manifested through kaolinite, illite, chlorite; carbonate lithologies are represented through calcite, aragonite, and dolomite; and evaporites are shown by as gypsum and anhydrite, in order to predict the reservoir temperature. However, fluid-mineral equilibrium condition is always calculated before predicting reservoir temperature.

3.3 Gas geochemistry studies

The study of geothermal gases emanating from thermal springs may provide more insights into the structural geology of a geothermal system (Bogie *et al.* 1987; Chiodini and Cioni 1989; Nicholson 1993). The geothermal gases are classified into two categories: one is reactive gas (steam, CO_2 , NH_3 , H_2S , N_2 , H_2 , CH_4 , CO) which depicts geochemical equilibrium and reveals the origin of the heat

source and the other one is non-reactive or inert gas (He, Ar, Rn, etc.) which identifies the source of any radioactive element inside geothermal reservoirs. Generally, high temperature high enthalpic geothermal systems are the pragmatic source of CO₂ and CO with minor contributions from NH₃, H₂S, N₂, H₂, and CH₄, while low-temperature medium enthalpic geothermal systems contain high concentration of N₂ and CH₄ over other CO₂ and H₂S (Mahon *et al.* 1980; Nicholson 1993). Furthermore, due to greater solubility of NH₃, and H₂S over CO₂ in water, according to Henry's law, these gases are seldom detected unless they are present in considerable quantities in the gas phase (Ellis 1962).

4. Results

4.1 Hydrogeochemical analysis

Most of the hot springs of Munger show higher surface temperature manifestation compared to the springs of Rajgir and Tapovan–Mohra areas of Bihar. The highest thermal manifestation is observed in Bhimband (around 65°C) followed by Sitakund (60°C), near Phillipskund (53°C) and springs of Rishikund areas (around 46°C). The physicochemical parameters determined in the water samples are listed in table 1. The pH of all thermal waters varies from near acidic to neutral range with values ranging from 5.15 to 6.75 for hot springs and 6.23 to 7.32 for cold springs. From the pH values, it can be elucidated that the alkalinity of water is primarily contributed by bicarbonate ions. The electrical conductivity (EC) of these thermal waters is less than 100 µS/cm at 25°C in hot springs of Bhimband, Rishikund, Bhurkha, and Siringrishi, while higher EC values are observed in thermal waters of Sitakund (hot spring: 352 µS/cm and cold spring: 863 µS/cm), Phillipskund (343 µS/cm), Near Ganga Kinare (383 µS/cm), Bhaduria Bhar (199 µS/cm) and near Kharagpur Lake (126 µS/cm). A higher value of EC manifests a higher concentration of dissolved ions (Dutta and Gupta 2022). The value of total dissolved solids (TDS) of thermal waters is less than 1000 mg/l (freshwater TDS) which suggests the geogenic origin of dissolved ions through rock–water interaction.

The existence of major cations follows the following trend: Ca²⁺ > Mg²⁺ > Na⁺ > K⁺ and major anions: HCO₃⁻ > Cl⁻ > SO₄²⁻. As reported earlier

also, the predominant radicals found here are SiO₂, HCO₃⁻, Cl⁻, Mg²⁺, and Ca²⁺ with SO₄²⁻ present below the detection limit to minor concentration in most of the hot springs (Gupta *et al.* 2017). The Piper diagram (figure 2) shows that thermal waters from different waters fall under similar geochemical characteristics. Most of the hot and cold spring waters of Munger fall in the zone of Ca–Mg–HCO₃ type water, except hot spring waters of Bhimband-2, 3 (HS-8, HS-9), and Siringrishi (HS-12), which are mostly mixed type water.

For trace elemental composition, minor amounts of Sr, Ba, Rb, Cs, Zn, and Mn are found. However, these values are higher than the respective elemental composition in cold spring waters. Large quantity of phosphate is found in hot springs of Bhimband, Bhaduria Bhar, Rishikund and near Ganga Kinare (concentration >100 µg/l). As per Environmental Protection Agency (EPA), maximum phosphorus level in reservoirs utilised for drinking water should not be higher than 25 µg/l, otherwise aquatic ecosystem will be affected and digestive problems may also happen if phosphate enriched water is consumed for a long period of time.

4.2 Analysis of geothermal gases

As per table S3 of ESI, the small presence of CO₂ in hot springs of Munger district, Bihar may be from the degradation of organic matter within Precambrian meta-sedimentary rocks of Munger at depth or in near-surface produce both CO₂ and CH₄. As the alkalinity of water samples is primarily contributed by bicarbonate ion over carbonate ion at acidic pH, the conversion of HCO₃⁻_(aq) to CO_{2(g)} on boiling may also add minor CO₂ concentration in gases. Hence, CO₂-enriched springs are the countersignature of the bicarbonate water-type thermal springs (Raymahashay 1988). The aquatic geochemistry, like pH and density along boiling point-depth relationships, is manipulated to some extent by the concentration of CO₂ in gas samples (Mahon *et al.* 1980). Neither any sulfurous odour is felt nor are any depositions of yellow sulfur or iron sulfides observed in the vicinity of hot springs, which furthermore rules out any likelihood of occurrence of H₂S in any hot springs. The simplest and most common primary alkane amongst the hydrocarbon series, methane (also called *marsh gas*) is observed in some gas samples, which could be due to the degradation of organic matter within

Table 1. Geochemistry of hot (HS) and cold (CS) springs of various localities of Munger of Bihar, India.

Sample ID	Location	Temp (°C)	pH	Sp. cond. at 25°C (µS/cm)	Total hardness (mg/l)	HCO ₃ ⁻ (mg/l)	Cl ⁻ (mg/l)	NO ₃ ⁻ (mg/l)	SO ₄ ²⁻ (mg/l)	Ca ²⁺ (mg/l)	Mg ²⁺ (mg/l)	Na ⁺ (mg/l)	K ⁺ (mg/l)	SiO ₂ (mg/l)	F ⁻ (mg/l)	PO ₄ ³⁻ (µg/l)	Sr (µg/l)	Rb (µg/l)	Ba (µg/l)	Charge balance
HS-1	Sitakund	60	6.75	352	156	141	30	8	23	40	13	19	2	6	<0.2	<50	132.98	2.67	42.06	+4%
HS-2	Rishikund-1	46	5.41	40	45	40	9	2	1	10	5	1	<1	35	<0.2	66	10.57	1.03	8.82	+3%
HS-3	Rishikund-2	38-39	5.7	41	50	32	16	2	1	18	1	1	1	32	<0.2	37	34.28	1.24	15.89	+3%
HS-4	Rishikund-3	43-44	5.46	39	45	34	14	2	2	12	5	1	<1	29	<0.2	50	21.74	1.00	11.29	+4%
HS-5	Rishikund-4	44-45	5.61	54	50	47	11	2	2	10	6	2	<1	31	<0.2	235	11.09	1.19	9.00	+1%
HS-6	Bhurkha	43	5.39	41	50	46	9	2	1	18	1	1	<1	34	<0.2	83	9.80	1.44	10.39	+2%
HS-7	Bhimband-1	64-65	5.44	38	70	44	12	2	15	22	4	1	<1	51	<0.2	178	9.21	1.41	10.39	+4%
HS-8	Bhimband-2	63	5.39	28	40	29	10	1	18	19	2	1	<1	45	<0.2	111	9.14	1.38	8.83	+2%
HS-9	Bhimband-3	63-64	5.37	29	65	34	13	2	16	8	11	1	<1	49	<0.2	803	24.58	0.39	8.18	+4%
HS-10	Kharagpur Lake	25	6.5	126	85	76	11	2	13	18	10	6	<1	38	0.3	80	59.86	23.61	14.71	+4%
HS-11	Bhaduria Bhar	36	6.41	199	120	130	16	2	2	30	11	4	6	48	<0.2	93	5.64	0.45	<5.00	+2%
HS-12	Sringnishi	30	5.15	30	30	18	12	3	1	8	2	1	<1	23	<0.2	60	106.80	2.70	36.61	+2%
HS-13	Near Phillipskund	53	6.49	343	170	170	28	6	2	44	14	12	2	45	<0.2	76	116.36	3.33	41.34	+4%
HS-14	Near Ganga Kinare	43-44	6.65	383	170	162	34	9	5	42	16	12	2	45	<0.2	216	10.57	1.03	8.82	+4%
CS-1	Near Sitakund	27	7.32	863	330	312	77	38	54	88	25	55	13	15	<0.2	<50	231.31	2.29	65.29	+3%
CS-2	Near Bhaduria Bhar	23	6.23	85	60	45	18	4	2	13	7	3	<1	15	<0.2	60	18.90	0.71	14.05	+4%

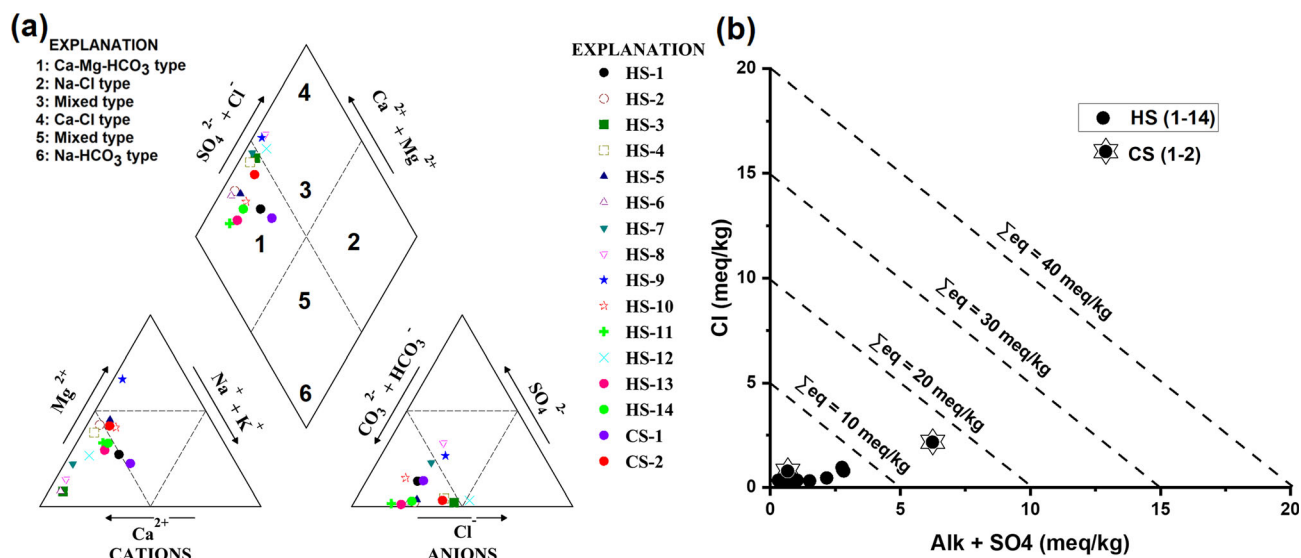


Figure 2. (a) Piper diagram manifesting types of thermal water with varying chemical constituents; (b) correlation diagram of Cl vs. alkalinity + SO₄ (meq/kg) (dotted lines represent iso-saline indices).

meta-sedimentary country rocks or decomposition of organic or biological materials by various anaerobic bacteria like *Methanobacterium*, *Methanococcus*, and *Methanospirillum*. Methane can also be produced by the reaction between CO₂ of carbonaceous materials and H₂ present in steam (Fischer–Tropsch reaction) (Panichi and Gonfiantini 1978; Nehring and D’Amore 1984). Being a light-weight and reactive gas with high escaping velocity, H₂ is primarily lost with time and reaction with neighbouring rock-forming minerals (Arnórsson *et al.* 1983). Hydrogen is observed only in the gas samples of Rishikund hot springs. Carbon monoxide is not observed in any gas samples. The high concentration of nitrogen (~90%) in gas samples further supports meteoric recharge waters of thermal springs over magmatic contribution, as it is the principal atmospheric gas occurring in nearly 77% of the earth’s atmosphere. Nitrogen could also be the carrier gas in the geothermal gas samples. The presence of a small quantity of air in all the gas samples (~10%) may be due to minor contamination from soil–air (Nicholson 1993). The inert gases like helium (He), neon (Ne), argon (Ar), krypton (Kr), xenon (Xe), and radon (Rn) are primarily contributed in the geothermal fluids through meteoric recharges. Amongst all the inert gases, He, Ar, and Rn are contributed through rock-leaching reactions too. In all the gas samples (except in Bhurkha-1), the occurrence of radiogenic helium has been observed. The highest concentration of helium is observed in gas emanated from hot spring Rishikund-1 with 553.32 mg/l. The presence

of radiogenic helium may be treated as the imprint of radioactive sources present in very low concentrations in thermal springs.

5. Discussions

5.1 Chemical evolution and major ion distribution of hot and cold spring waters

The placement of most of the data points representing various thermal waters in the same region of diamond plot in Piper diagram (figure 2a) indicates that different thermal sites encounter similar geochemical processes which control their water chemistry. The groundwater in such case is considered as the derivative of meteoric recharge, which either has diluted the hot spring waters a lot or aquifer rocks have minimally interacted with hot spring waters. Such minimal rock–water interaction, preventing dissolution of solutes in thermal waters, could possibly be due to silica scaling or coating of silica and calcite in the hydrothermal vents or channels which prevent aquifer rocks to react less with hot water resulting poor diffusion of rock forming elements in thermal water. In such case also, thermal water will be dilute or lower ionic content. The two thermal springs of Bhimband (HS-7 and HS-8) have identical Na/K, Na/Ca, and Cl/HCO₃ values suggesting that these springs are the outlets of the same geothermal reservoir. Similar behaviour of springs is also observed by Singh *et al.* (2020). The cold springs of Munger arise from the alluvium formation.

To gain further insights regarding water classification parameter, total ionic salinity (TIS: $\sum \text{eq}$) of hot spring water samples has been evaluated (Apollaro *et al.* 2019, 2020). Here, Cl^- ion concentration is plotted against total concentration of alkalinity and SO_4^{2-} ion to get a correlation diagram (figure 2b). Here, concentrations of relevant ions are taken in milliequivalents per kilogram (meq/kg). The correlation plot manifests low salinity condition of thermal waters with isoTIS value <10 meq/kg. Only in one cold spring sample (CS-1), due to greater concentration of Na^+ and Cl^- ions, the TIS has increased up to 7 meq/kg, which is <20 meq/kg isoTIS line. However, as the values of TIS are very low, it suggests that these geothermal circuits are being recharged by meteoric waters with a limited extent of water-aquifer rock interaction (Arnórsson *et al.* 1983).

The ion-exchange processes may move water from Ca–Mg– HCO_3 domain to mixed water type. The fact can be exemplified through calculating chloro-alkaline indices (CA) whose positive value indicates ion-exchange of Na^+ and K^+ in water with Ca^{2+} and Mg^{2+} of aquifer rocks and negative value indicates the reverse process (Schoeller 1977). The source of Na^+ and K^+ content in water could be due to continuous reuse/cycling of groundwater. For the thermal and non-thermal waters of Munger, all the CA values are positive with CA-1 value ranging between 0.3 and 0.9 and CA-2 value ranging between 0.045 and 0.482 confirming cation-anion exchange reaction where Na^+ and K^+ in water with Ca^{2+} and Mg^{2+} of aquifer rocks causing water-type to be Ca–Mg– HCO_3 type as evident from Piper diagram.

The fact that the host rocks are the primary sources of dissolved ions in hot and cold spring waters, is further confirmed from Gibbs diagram (Gibbs 1970), where total dissolved solids of thermal waters are plotted against $\text{Na}^+ / (\text{Na}^+ + \text{Ca}^{2+})$ and $\text{Cl}^- / (\text{Cl}^- + \text{HCO}_3^-)$ (figure S1 of ESI). The diagrams reveal the ideas about the source of relative ionic strength/concentration which could either be from rock weathering by water–rock interaction or by precipitation/evaporites dominance or by saline water mixing. As per figure S1 of ESI, the Gibbs diagram reveals that the clustering of points in the case of major cations plot for thermal waters of Munger around rock dominance region is due to rock weathering by *in situ* host rock–water interactions occurring in deep reservoir. The diagram further depicts that for major anions, majority of points cluster in the boundary

of precipitation dominance and rock dominance regions, leaning more towards precipitation dominance region, suggesting that anion concentration is controlled largely by meteoric water recharge than host rock–water interactions in the deep reservoir. This diagram further clarifies the mixing of thermal water with meteoric water, which percolates through faults, fractures, and lineaments into the deep reservoir and gets heated up due to convection heat waves and vents as thermal springs.

Hence it is elucidated from the Gibbs diagram and CA values that ion sources in hot and cold spring waters are predominantly governed through aquifer rock–water interactions. Now, to get insights about variation in the chemical composition of cations and anions in water, a Stiff's diagram is drawn (Stiff 1951). Here, the width of the polygon reflects approximate total ionic content in the water samples (Hem 1985; Hounslow 1995). To study the relative distribution of cations and anions in thermal springs, we have divided the thermal springs into three groups: *Group-A*, Sitakund, Phillipskund, and Ganga Kinare springs; *Group-B*, Bhimband group of springs; and *Group-C* Rishikund, Bhurkha and Bhaduria Bhar springs (figure S2 of ESI). The sizes of the polygon are different for various thermal springs suggesting their uneven ionic distribution patterns. The varied ionic concentrations for a different group of thermal springs suggest a divergent extent of diffusion of mineral forming elements in rocks through rock–water interaction at various reservoir temperatures of thermal springs. However, as the ionic concentration is low, it could also be possible that the thermal springs are being recharged from the same source (Shah *et al.* 2021). Hence, as per Stiff's plot, 81% of the thermal spring water of Munger is of Ca–Mg– HCO_3 type and 19% of the thermal spring water of Munger is mixed type.

Understanding the source of the dissolved solutes in thermal and non-thermal waters depends heavily on geochemical evolution, as their concentrations are primarily determined by extent of water–rock interactions, aquifer geology, residence time of water, extent of dilution with meteoric water or groundwater, salt-water intrusion, etc. (Mukherjee and Fryar 2008; Chatterjee *et al.* 2022). Bivariate scatter plots between Na-normalised Mg and Na-normalised HCO_3 with Na-normalised Ca in micromolar concentration (figure 3) illustrate the role of various agencies in determining solute concentration in groundwater (Mukherjee and Fryar 2008).

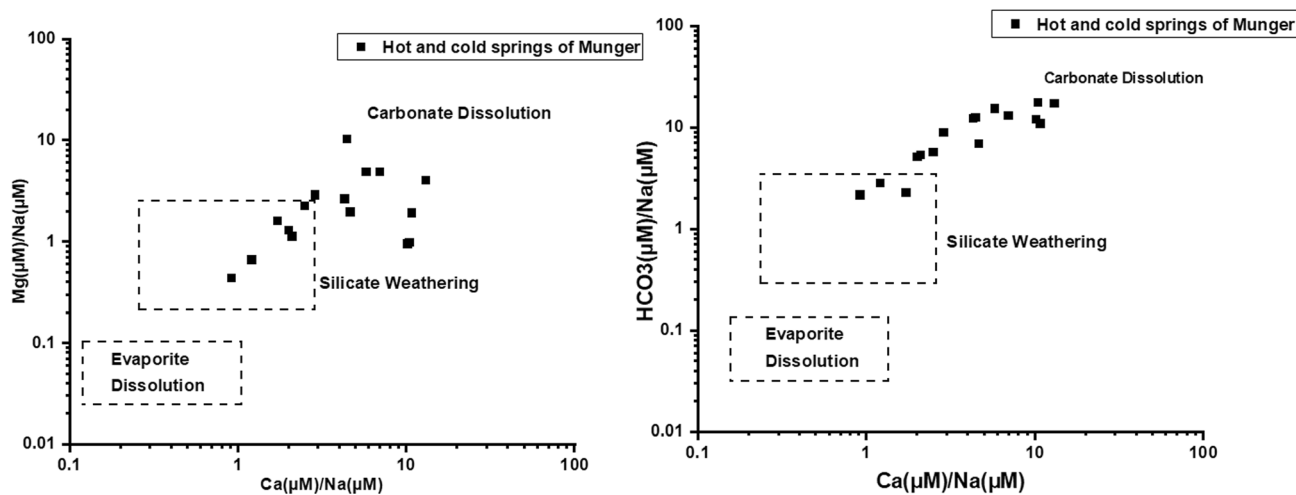


Figure 3. Bivariate scattered plots of Na-normalised Ca with Na-normalised Mg ($\mu\text{M}/\mu\text{M}$) and Na-normalised HCO_3 ($\mu\text{M}/\mu\text{M}$) to show processes of origin of solutes in water. The dashed areas show global average compositions of groundwater with respect to different weathering mechanisms.

Table 2. Saturation indices of water samples of the study area with respect to relevant minerals.

Sample no.	Aragonite	Calcite	Dolomite	Chalcedony	Quartz	$\text{SiO}_2(\text{a})$	Log pCO_2	Talc
HS-1	-0.74	-0.60	-1.34	-0.45	-0.02	-1.29	-1.77	-5.69
HS-2	-1.79	-1.65	-3.26	0.32	0.75	-0.52	-2.30	-3.64
HS-3	-1.64	-1.49	-3.90	0.28	0.71	-0.56	-2.40	-5.89
HS-4	-1.79	-1.65	-3.33	0.23	0.66	-0.61	-2.37	-3.97
HS-5	-1.73	-1.59	-3.06	0.26	0.69	-0.58	-2.23	-3.63
HS-6	-1.48	-1.34	-3.59	0.30	0.73	-0.54	-2.24	-5.79
HS-7	-1.44	-1.30	-2.99	0.48	0.91	-0.36	-2.26	-3.35
HS-8	-1.67	-1.53	-2.44	0.43	0.85	-0.41	-2.44	-4.45
HS-9	-1.99	-1.84	-3.21	0.46	0.89	-0.38	-2.37	-2.09
HS-10	-1.30	-1.16	-2.24	0.35	0.78	-0.49	-2.03	-2.70
HS-11	-0.87	-0.73	-1.54	0.45	0.88	-0.39	-1.80	-2.21
HS-12	-2.22	-2.08	-4.41	0.13	0.56	-0.71	-2.64	-5.52
HS-13	-0.62	-0.47	-1.10	0.43	0.86	-0.41	-1.69	-2.07
HS-14	-0.66	-0.52	-1.11	0.43	0.86	-0.41	-1.71	-1.90

These agencies include carbonate hard-rock dissolution, weathering of silicate minerals, and evaporite dissolution. From both the plots, it is clearly illustrated that datasets representing thermal waters lie close to the silicate weathering zone manifesting its primary role in controlling total ion concentration in waters. The fact is also supported by studying the regional geology and mineralogy of the study area where primary rock types are quartzite and phyllite.

5.2 Mineral saturation states (SI) studies

The incongruent dissolution of minerals results in the precipitation of minerals in thermal waters. The hot spring waters of Munger decipher saturation with respect to minerals of silica, i.e.,

chalcedony and quartz, while undersaturation with respect to calcite, aragonite, dolomite, and amorphous silica (table 2). The thermal waters have chalcedony and quartz at or just above the equilibrium line, and therefore, high temperature features the saturation point of minerals. With the rise of temperature, thermal waters get more saturated with calcite, dolomite and talc minerals. At the same time, the rise of temperature with depth promotes a greater degree of undersaturation of silica minerals like chalcedony, quartz and amorphous silica. The fact is illustrated by studying the temperature-dependent mineral saturation indices studies of two representative thermal water samples: HS-7 (Bhimband-1) and HS-11 (Bhaduria Bhar) (figure 4). The presence of CO_2 in hot spring

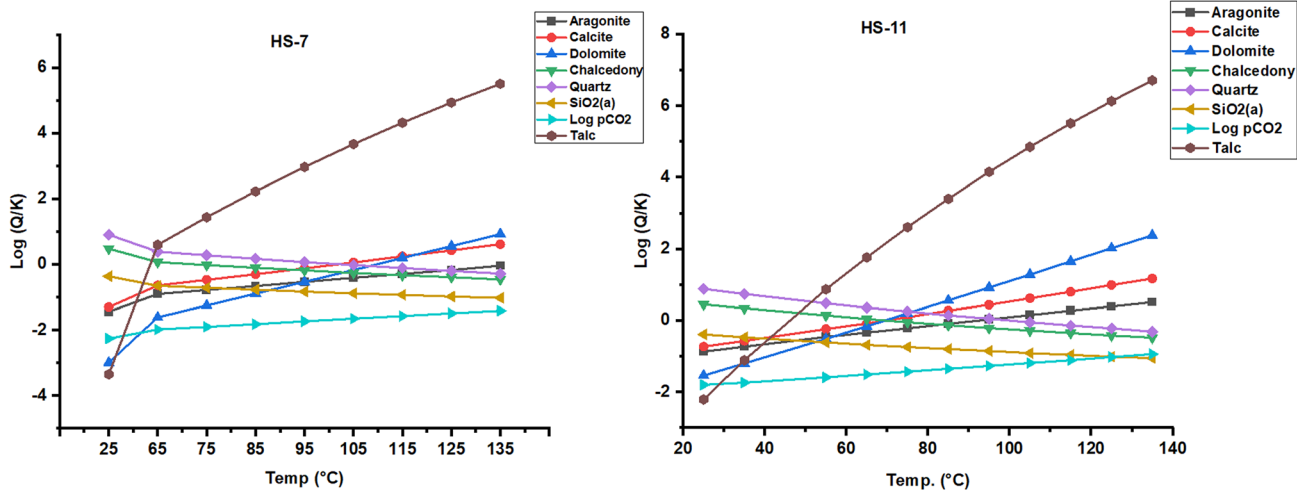


Figure 4. Log(Q/K) vs. temperature plot of different mineral phases for hot springs HS-7 and HS-11.

gas samples may suggest its dissolution with rise of temperature at atmospheric pressure, which ultimately lowers the pH of the medium, thus resulting in more solubility of calcite mineral in the discharge areas (Shestakova *et al.* 2018).

5.3 Na–K–Mg and Cl–SO₄–HCO₃ ternary diagrams

For Na–K–Mg ternary diagram, most of the points are shifted towards the Mg vertex, suggesting either mixing of Mg-enriched rich groundwater in geothermal fluids or leaching of secondary Mg-containing rock-forming minerals during fluid–rock interaction. All the waters are immature in nature and lie far below the partial equilibrium zone (figure 5a). The thermal waters of Sitakund, Phillipskund, and Ganga Kinare have nearly uniform Na/K ratios suggesting that the springs are fed by the same reservoir (table 1) (Fournier and Truesdell 1974). The poor content of alkali metals in the geothermal fluids of Munger restricts it from predicting reservoir temperature using multi-component cation geothermometry (Giggenbach 1984, 1988). Due to the intense mixing of shallow groundwater with geothermal waters, the fluid composition is affected and hence prolonged geological time is required to achieve mineral-solution equilibrium.

The fast-ascending geothermal fluids are vital to understanding the characteristics of reservoir behaviour, its temperature, and the surrounding geology of hot springs (Singh *et al.* 2020). In highly geo-pressurised systems at an elevated temperature, the thermal waters react spontaneously with

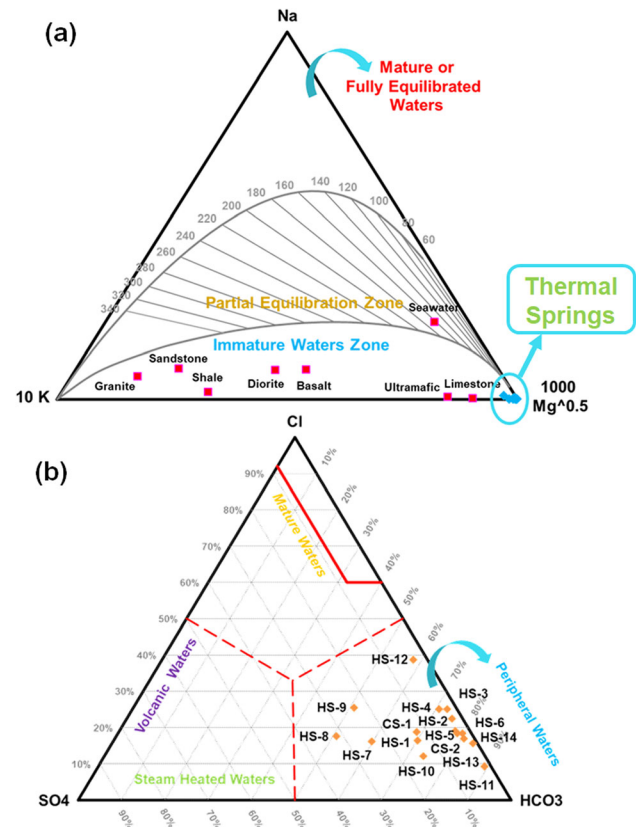


Figure 5. (a) Na–K–Mg and (b) Cl–SO₄–HCO₃ triangular plots unveiling the nature of geothermal waters of Munger.

neighbouring host rocks and get saturated slowly due to diffusion or leaching of rock-forming solutes into thermal fluids and slowly move towards the equilibration zone (Giggenbach 1988). Hence, hydrogeochemical analysis of these fluids provides valuable information regarding underground deep thermal processes. As per the Cl–SO₄–HCO₃

ternary plot, all the thermal waters are peripheral/immature in nature, with meteoric in origin having predominance in bicarbonate ion concentration (figure 5b). The thermal water of Siringrishi, though peripheral in nature, lies close to the boundary of mature and immature water, which suggests a greater propensity of thermal water to achieve maturity by rock–water interaction compared to other thermal waters. As SO_4^{2-} concentration is low in most of the thermal springs; it manifests that the thermal waters are not derived from volcanic condensates, i.e., near-surface condensation of volcanic gases into meteoric waters does not occur.

5.4 Reservoir temperature and direct utilisation of geothermal waters

As per the placement of thermal water samples in Cl– SO_4 – HCO_3 ternary plot in peripheral water region suggests that the waters are immature enough and still have not attained geochemical equilibrium. A similar fact is also established from Na–K–Mg ternary diagram, which suggests that thermal waters lie in immature water domain. Hence, these thermal waters must be used with caution for determining reservoir temperature of hot springs. The thermal waters of the study area are more bicarbonate rich and dilute chloride type (HCO_3 , Cl type water) and such waters provide ideas about sub-surface processes occurring in shallow depths (Nicholson 1993; Cioni and Marini 2020). Furthermore, due to the intense mixing of thermal waters with cold groundwater, the use of cation exchange geothermometry is restricted as there exists a high chance of intrusion of cations from surrounding cold groundwater too. Thus, cation geothermometry cannot be used for correct reservoir temperature estimation.

The thermal springs of Bihar emerge through Precambrian meta-sediments bearing quartzite and phyllite rocks channelled by huge fractures and joint systems, quartz is the only mineral that may be assumed to be in geochemical equilibrium with the thermal water as it is in constant interaction with water (Guha 1970; Pandey and Raymahashay 1981; Ahmed and Wanjari 2009). Further, quartz and chalcedony are the only minerals which are saturated in thermal waters, with degree of saturation lying just above the equilibrium line. The studies of hydrothermal alteration in previously explored geothermal areas have revealed that

quartz is an important secondary mineral at relatively shallow depth (Muffer and White 1968). The reservoir temperature obtained from quartz conductive geothermometer (procuring maximum steam loss) ranges between 69° and 103°C and from quartz adiabatic geothermometer (procuring no steam loss) ranges between 74° and 103°C. The high consistencies between two quartz geothermometers indicate that quartz geothermometry can be confidently applied for the estimation of reservoir temperatures of thermal springs of Munger (table S1 of ESI).

High solubility of chalcedony in thermal water at low temperature is due to its fine particle size, and larger effective surface area. This could probably be the sufficient reason behind the manifestation of the lower reservoir temperature of the thermal springs estimated from the chalcedony geothermometer. Also, as the thermal springs of Munger have slow discharge rates with the high lateral flow, it is possible that precipitation of silica can occur during the transit of thermal waters to the surface, resulting in lower reservoir temperature values. Furthermore, the compositions of cold spring waters near Sitakund and Bhaduria Bhar are comparatively similar to that of hot spring waters, suggesting either slower dissolution of rock-forming minerals in thermal water through rock–water interaction or lower residence time of thermal water under thermo-artesian conditions. Relatively higher concentrations of calcium ions may arise partly from the greater dissolution of calcite and dolomite in thermal water present in country rocks, as confirmed from SI studies also at elevated temperatures. Complete disharmony between the temperatures evaluated from quartz geothermometry and Na–K geothermometry is observed. This anomaly may be due to the fact that Na–K ion exchange reactions happen at high temperature, pressure and at high depth, which is not the case for thermal waters of Munger.

The estimated reservoir temperatures in Munger thermal springs specify the localities as low enthalpy geothermal resource whose thermal waters can be used for aquaculture, balneotherapy, dehydration of fruits and vegetables using greenhouse heating techniques, etc. (Chandrasekharam *et al.* 2006). The direct use of geothermal waters for heating purpose can effectively reduce the CO_2 emission into the environment. Given the estimated reservoir temperature of thermal springs lying between 74° and 103°C, the thermal waters (specially Bhimband, Phillipskund, Sitakund, etc.)

can be utilised in power generation purpose using ORC (organic Rankine cycle) technique using binary cycle technique (Chandrasekharam and Bundschuh 2008). The cumulative discharge rates of thermal springs of Bhimband and Sitakund-Phillipskund are 7.9 and 6.5 L/s, respectively, which may support power generation using ORC technique.

5.5 *Mixing model and enthalpy-chloride diagram*

The deep thermal waters get mixed with meteoric water or cold groundwater at shallow depth, before getting discharged as geothermal springs, rendering the springs to be less saline and more dilute with total dissolved solids, and this process is called *dilution* of geothermal fluids. For interpreting the chemistry of mixed geothermal fluids, it is vital to estimate their degree of dilution, and on this stand-point, enthalpy *vs.* chloride mixing models have found widespread usage. For interpreting mixing or dilution confidently, a group of thermal springs should be considered rather than focussing on the chemistry of individual springs with a further correlation of the results with the spatial distribution of springs (Arnorsson 1985).

Enthalpy-chloride diagrams are useful in understanding the hydrogeology of any geothermal system as it provides insights into various sub-surface processes like boiling, dilution-mixing, conductive-cooling, steam-heating of waters, etc. (Nicholson 1993; Singh 2020). They provide information on the extent of mixing of hot-spring waters or re-equilibration in a reservoir at shallow depth, which is not possible by the simple application of an absolute geothermometer (Truesdell and Fournier 1977). Quartz geothermometer is an absolute concentration-dependent chemical geothermometer and is intensely affected by boiling and dilution of springs. Furthermore, the solubility of quartz is also not a linear function of temperature as its solubility rapidly increases with temperature and becomes maximum at 250°C; beyond which it gets precipitated into the medium and gets separated from thermal water. As the thermal springs of Munger are classified as low enthalpic geothermal resources type with reservoir temperature near 100°C, quartz mostly remains in soluble state in thermal water (Shukla 1981; Razdan *et al.* 2008). However, its concentration is significantly affected with dilution by neighbouring shallow groundwater. As per

figure S3 of ESI, quartz geothermometer enthalpy at a steam point is plotted at 2775 kJ/kg as this value is valid for most situations irrespective of reservoir depth (Truesdell and Fournier 1977; Arnorsson 1985). In this figure, all the data points are situated at extreme left in meteoric water box under boiling spring line having maximum enthalpy <500 kJ/kg with the highest enthalpic water recorded in Bhimband hot spring water (435 kJ/kg) suggesting that thermal waters of Munger are meteoric in origin with medium enthalpy and dilute chloride type. Under such circumstances, it is vital to access the percentage of cold water mixing with hot springs for further rationalisation of the extent of dilution. For this, we have also divided thermal waters of Munger into three groups of springs, like in Stiff's plot: Group-A consisting of Sitakund, Phillipskund, and Ganga Kinare thermal springs; Group-B consisting of Bhimband group of springs; and Group-C consisting of Rishikund, Bhurkha and Bhaduria Bhar springs (figure 6). Fournier and Truesdell (1974) established empirical equations (equations 1 and 2) to demonstrate the extent of mixing of cold spring water with geothermal water considering non-reactive silica contents and temperature of hot and cold springs (Fournier and Truesdell 1974). The two equations can be solved graphically as silica content and temperature of geothermal spring are independent mathematical functions of the original hot spring component. However, an assumption is made regarding consideration of enthalpy of water below 100°C which is numerically equal to the temperature of water.

$$X_t = \frac{H_{\text{hot}} - H_{\text{spring}}}{H_{\text{hot}} - H_{\text{cold}}} \quad (1)$$

$$X_{Si} = \frac{S_{i_{\text{hot}}} - S_{i_{\text{spring}}}}{S_{i_{\text{hot}}} - S_{i_{\text{cold}}}} \quad (2)$$

where X_{Si} and X_t are the fractions of cold-water components mixed with the hot spring at a particular reservoir temperature ($t^\circ\text{C}$), H_{spring} and $S_{i_{\text{spring}}}$ are the respective enthalpy and silica content of hot springs and H_{cold} and $S_{i_{\text{cold}}}$ are the respective enthalpy and silica content of cold springs, and H_{hot} and $S_{i_{\text{hot}}}$ are the respective enthalpy and silica solubility content values as a function of temperature obtained after Fournier and Truesdell (Fournier and Truesdell 1974) (table S2 of ESI).

On graphically representing the data sets in two-dimensional plots between temperatures of

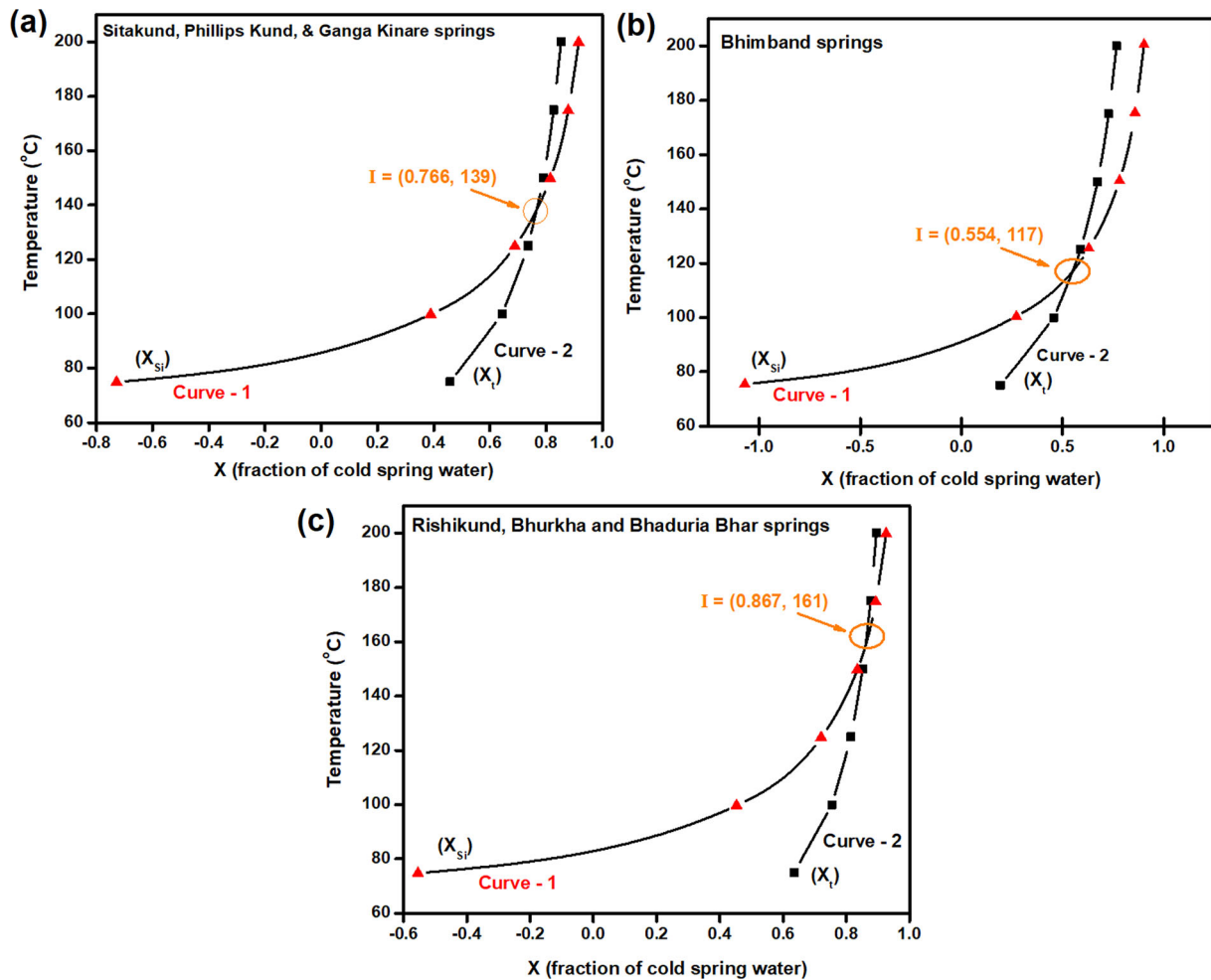


Figure 6. Hot and cold spring water fractions in various groups of mixed water thermal springs in Munger, Bihar.

vent *vs.* fraction of cold-water component in hot spring elucidated a particular intersection point of X_{Si} and X_t for each group of thermal springs. For Group-A springs, the curves intersected at $X = 0.766$ and $t = 139^\circ\text{C}$, which suggests that the Sitakund group of springs of Munger have 76.6% cold meteoric water intrusion with 23.4% of deep hot spring water at reservoir temperature 139°C . Similarly, for group B and C thermal springs, 55.4% and 86.7% of cold meteoric water are mixed with 44.6% and 13.3% deep hot spring water at reservoir temperature 117° and 161°C , respectively. Shukla (1981) reported that Bhimband hot spring, in the Rajgir–Munger belt, is consisted of nearly 30.7% of hot spring water and 69.3% of cold spring water at a reservoir temperature of 150°C (Shukla 1981). As the calculation is based on silica content in thermal water, the deviation in the composition of cold meteoric water in thermal water of Bhimband group of springs may be due to the presence of other

polymorphs of silica like crystabolite, chalcedony, quartz, etc., which have variable solubilities at different temperature.

The $\delta^{18}\text{O}$ *vs.* δD isotopic study in thermal waters by Sharma *et al.* (1970) and Bhattacharya *et al.* (1985) suggests that recycled meteoric water is the origin of thermal waters of Rajgir–Munger, while tritium ($\delta^3\text{H}$) studies by Gupta and Sukhija suggest shallow circulation of thermal waters and intense mixing with meteoric water as tritium values of thermal waters are close to the observed tritium values of meteoric waters (Gupta and Sukhija 1974; Raymahashay 1988). Hence, as illustrated from our studies, the thermal waters of Munger consist of deep circulating meteoric water (bearing lower concentration of dissolved solids) as a major component with a minor contribution from hot component (enriched with dissolved solids), causing intense dilution in resultant fluids, along with various gaseous manifestations (Pandey *et al.* 1970).

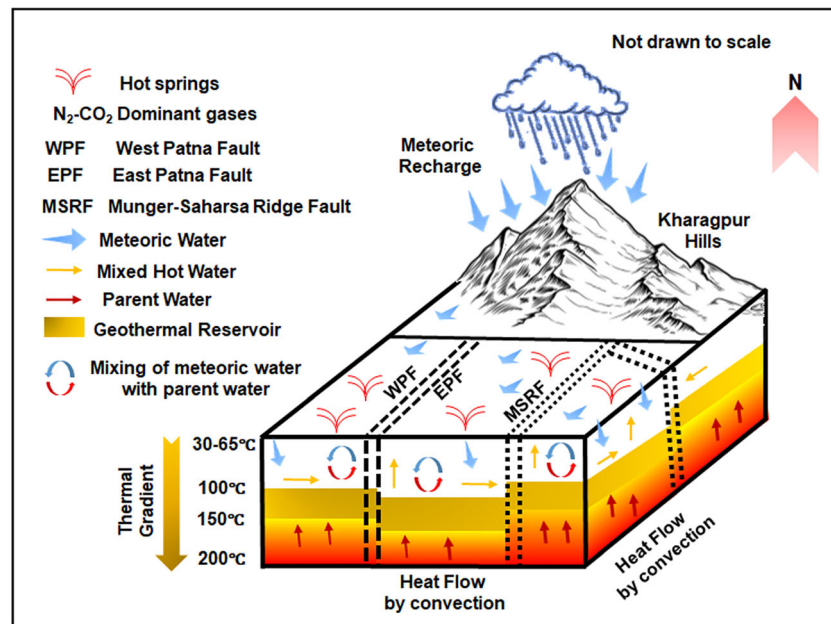


Figure 7. A conceptual hydrogeochemical evolution model for the present geothermal study area.

5.6 Conceptual model

Considering the structural and regional geological landscape of Munger geothermal province and reported isotope studies by Sharma and Bhattacharya, a conceptual hydrogeochemical model has been proposed (figure 7). The present geothermal system is located on the northern side of the Chhotanagpur–Granitic Gneissic Complex along the MSR fault zone in the foothills of Kharagpur hills where MSR and EPF fault/fracture zones provide thrusts and channels for water flow. Detailed $\delta^{18}\text{O}$ vs. δD isotopic study in thermal waters by Sharma and Bhattacharya suggested that the thermal waters of Munger are primarily meteoric in origin, which percolate deep underground through various fault/fractures and permeable zones in rock and get heated up at a certain depth due to the high geothermal gradient of the study area and heat flow by deep-seated convective currents and ultimately ascend as thermal water in the upflow zone with discharge temperature varying between 25 to 65°C. These normal faults regulate the near-surface conduits for the circulating waters in such hydrothermal-convection systems. The thick Rajgir–Munger meta-sedimentary groups of rocks over intrusive granites (as an extension of SONATA lineament) act as a thermal blanket which traps heat in relatively shallow aquifers. The thermal waters in these aquifers likely originate from leakage away from fault conduits (Mariner *et al.* 1983). During

ascending, the thermal waters get mixed up with shallow groundwater and rainwater, thereby getting diluted which is manifested through lower electrical conductivity values. The thermal waters of Munger are slow ascending with the lateral flow, which further enhances the chances of mixing thermal waters with local groundwater at shallow depths as evaluated from their slow discharge rates. It is also revealed from mixing modelling plots done in the present study that the thermal waters are highly diluted and mixed up with cold spring water. The variation in discharge temperature also implicates the role of bicarbonate type of water of thermal springs in mixing processes and the waters are immature in nature and yet to achieve geochemical equilibrium. Hence, the present geothermal system of near peninsular India is predominantly a fault-driven low-temperature medium enthalpic zone, with an intense dilution of thermal waters bearing subsurface reservoir temperature around 100°C.

6. Conclusions

In the present study, we have conducted a comprehensive analysis focussing only on hot springs of Munger, Bihar along Munger–Saharsa Ridge Fault zone to better comprehend reservoir features of thermal springs. Majority of thermal springs are identified as Ca–Mg– HCO_3 type, except Bhimband-2, 3, and Siringrishi thermal springs, which

are predominantly mixed water types, and different scatter plots show multiple geochemical mechanisms controlling the geochemistry of waters. The waters are peripheral/immature in nature and meteoric in origin, receiving heat neither from any volcanic condensates nor from any steam-heated groundwater. High lateral flow and slow discharge rate of thermal springs enhance the chance of dilution or mixing of thermal springs with meteoric water. Analysis of Gibbs diagram and bivariate plots reveal that weathering of silicate rock minerals is the primary source of evolution of solutes in thermal waters, with high ion-exchange processes as confirmed from chloro-alkaline values. The study shows that mixing mechanisms with shallow groundwater or rain, and gas–water–rock interaction may be the primary contributing factors dictating the water chemistry of Munger hot springs. The study suggests that Rishikund, Bhurkha, and Bhaduria Bhar springs are most diluted with groundwater/rain over Bhimband and Sitakund group of hot springs, contributing the highest percentage of cold-water intrusion (76.6%) in hot fluids (23.4%).

Our study further elaborated that these thermal waters are saturated with silica minerals but are undersaturated with calcite, dolomite and talc minerals near surface; however, degree of saturation of the undersaturated minerals increases with increase of reservoir temperature. As silica minerals saturation is just above the equilibrium point and the regional geology of the study area is composed of quartzite and phyllite rock, whose primary mineral component is silica, quartz geothermometry is suitable for reservoir temperature estimation over multi-component cation geothermometry. Quartz geothermometry predicts reservoir temperature of thermal springs of $\sim 100^{\circ}\text{C}$ with maximum temperature recorded for Bhimband hot spring of 103°C and 435 kJ/kg enthalpy as evaluated from enthalpy–chloride mixing models. The study thus suggests low enthalpic geothermal resource of the area. Analysis of geothermal gases of thermal springs provides information about the predominance of $\text{N}_2\text{--CO}_2$ type gases.

Based on all the facts, a pen-picture of the hydrogeochemical model has been drawn conceptually, which depicts a way of recharge, mixing of waters/dilution, source of heating, equilibration with the host rock, CO_2 release during the ascent of waters, and discharge of waters as thermal springs. The detailed structural geology studies manifest Munger geothermal system as a fault-controlled

geothermal zone that provides insights on fluid circulation, storage, and upsurge of geothermal waters. It is the existing fault systems of the study area that facilitate a deeper circulation of rainwater. The residence time of thermal waters in the geothermal aquifer is short for any substantial host rock–water interactions which could be a possible reason for extremely lower dissolved total ion content. The thermal insulation provided by thick meta-sedimentary groups of rocks over intrusive granites, as an extension of SONATA lineament, make the study area one of the promising geothermal systems in India. However, more geophysical or magnetotelluric studies are required, mainly on Bhimband thermal spring as this spring has sufficient potential to express itself as a geothermal energy resource in the future.

Acknowledgements

The authors would like to thank all the officers and staff members of the Geological Survey of India, Northern Region Lucknow, who were associated with this project for their active co-operation in this study. AD acknowledges Dr Apratim Kumar Rai (Sr. Geologist) and Dr Abhisek Gupta (Sr. Chemist) for map construction and worthwhile suggestions. The authors are extremely grateful to the Additional Director General and HOD (NR), Geological Survey of India, Lucknow, for inspiration. Authors highly acknowledge the painstaking efforts taken by the associate editor and learned reviewer for constantly providing highly constructive suggestions for improving the manuscript.

Author statement

AD and AP designed and convinced the idea. Data from the field has been collected by AD and RKG under the supervision of AP. All authors contributed to the writing of the manuscript and its interpretations.

References

- Ahmed M and Wanjari N 2009 Volcano-sedimentary sequence in the Munger–Rajgir metasedimentary belt, Gaya district, Bihar; *Indian J. Geosci.* **63**(4) 351–360.
- APHA (American Public Health Association) 1985 Standard methods for the examination of water and waste water; 6th edn, APHA, Washington, DC.

- Apollaro C, Tripodi V, Vespasiano G, De Rosa R, Dotsika E, Fuoco I, Critelli Sa and Muto F 2019 Chemical, isotopic and geotectonic relations of the warm and cold waters of the Galatro and Antonimina thermal areas, southern Calabria, Italy; *Mar. Pet. Geol.* **109** 469–483, <https://doi.org/10.1016/j.marpetgeo.2019.06.020>.
- Apollaro C, Caracausi A, Paternoster M, Randazzo P, Aiuppa A, De Rosa R, Fuoco I, Mongelli G, Muto F, Vannia E and Vespasiano G 2020 Fluid geochemistry in a low-enthalpy geothermal field along a sector of southern Apennines chain (Italy); *J. Geochem. Explor.* **219** 106618, <https://doi.org/10.1016/j.gexplo.2020.106618>.
- Arnórsson S 1985 The use of mixing models and chemical geothermometers for estimating underground temperatures in geothermal systems; *J. Volcanol. Geotherm. Res.* **23(3–4)** 299–335, [https://doi.org/10.1016/0377-0273\(85\)90039-3](https://doi.org/10.1016/0377-0273(85)90039-3).
- Arnórsson S, Gunnlaugsson E and Svavarsson H 1983 The chemistry of geothermal waters in Iceland. III. Chemical geothermometry in geothermal investigations; *Geochim. Cosmochim. Acta* **47** 567–577, [https://doi.org/10.1016/0016-7037\(83\)90278-8](https://doi.org/10.1016/0016-7037(83)90278-8).
- Bhattacharya S K, Gupta S K and Krishnamurthy R V 1985 Oxygen and hydrogen isotopic ratios in ground waters and river waters from India; *Proc. Indian Acad. Sci. (Earth Planet. Sci.)* **94** 283–295, <https://doi.org/10.1007/BF02839206>.
- Bogie I, Lawless J V and Pornuevo J B 1987 Kaipohan: An apparently non-thermal manifestation of hydrothermal systems in the Philippines; *J. Volcanol. Geotherm. Res.* **31** 281–292, [https://doi.org/10.1016/0377-0273\(87\)90072-2](https://doi.org/10.1016/0377-0273(87)90072-2).
- Chandrasekharam D and Bundschuh J 2008 *Low-enthalpy geothermal resources for power generation*; CRC Press.
- Chandrasekharam D and Prasad S R 1998 Geothermal system in Tapi rift basin, northern Deccan province, India; In: *Proceedings 9th water-rock interaction* (eds) Arehart G B and Hulston J R, A. A. Balkema, Leiden, The Netherlands, pp. 667–670.
- Chandrasekharam D, Chandrasekhar V and Alam M A 2006 Geothermal energy resources of India: Ongoing and future developments; In: *American Association of Petroleum Geologists Conference Proceedings*, pp. 5–8.
- Chatterjee N and Ghose N C 2011 Extensive Early Neoproterozoic high-grade metamorphism in North Chhotanagpur Gneissic Complex of the Central Indian Tectonic Zone; *Gondwana Res.* **20(2–3)** 362–379, <https://doi.org/10.1016/j.gr.2010.12.003>.
- Chatterjee S, Dutta A, Gupta R K and Sinha U K 2022 Genesis, evolution, speciation and fluid-mineral equilibrium study of an unexplored geothermal area in Northeast Himalaya, India; *Geothermics* **105** 102483, <https://doi.org/10.1016/j.geothermics.2022.102483>.
- Chiodini G and Cioni R 1989 Gas geobarometry for hydrothermal systems and its application to some Italian geothermal areas; *Appl. Geochem.* **4** 465–472, [https://doi.org/10.1016/0883-2927\(89\)90004-8](https://doi.org/10.1016/0883-2927(89)90004-8).
- Cioni R and Marini L 2020 A thermodynamic approach to water geothermometry; *Geochemistry*, <https://doi.org/10.1007/978-3-030-54318-1>.
- Das B 1967 On the lithological sequence and overall structure of the rocks around Rajgir, Bihar; *Bull. Geol. Soc. India* **4(2)** 46–49.
- Dutta A and Gupta R K 2022 Geochemistry and utilisation of water from thermal springs of Tawang and West Kameng Districts, Arunachal Pradesh; *J. Geol. Soc. India* **98** 237–244, <https://doi.org/10.1007/s12594-022-1964-7>.
- Dutta A, Gill G K S and Srinivasan J 1982 Geology and geochemistry of hot springs located in Subansiri Valley, Subansiri district of Arunachal Pradesh; *Special Publication 8(III)* 137–144.
- Ellis A J 1962 Interpretation of gas analysis from the Wairakei hydrothermal area; *NZJ Sci.* **5** 434–452.
- Fournier R O 1977 Chemical geothermometers and mixing models for geothermal systems; *Geothermics* **5** 41–50, [https://doi.org/10.1016/0375-6505\(77\)90007-4](https://doi.org/10.1016/0375-6505(77)90007-4).
- Fournier R O and Truesdell A H 1974 Geochemical indicators of subsurface temperature. Part 2: Estimation of temperature and fraction of hot water mixed with cold water; *J. Res. US Geol. Surv.* **2** 263–270.
- Gautam A, Rai S C and Shekhar R 2018a Hot-springs of Rajgir: Spatial re-distribution and conservation; *Sree Journal of Spatial Perspectives* **2(1)** 1–9.
- Gautam S K, Tziritis E, Singh S K, Tripathi J K and Singh A K 2018b Environmental monitoring of water resources with the use of PoS index: A case study from Subarnarekha River basin, India; *Environ. Earth Sci.* **77** 70, <https://doi.org/10.1007/s12665-018-7245-5>.
- Gibbs R J 1970 Mechanism controlling world water chemistry; *Science* **17** 1088–1090, <https://doi.org/10.1126/science.170.3962.1088>.
- Giggenbach W F 1984 Mass transfer in hydrothermal alteration systems – A conceptual approach; *Geochim. Cosmochim. Acta* **48** 2693–2711, [https://doi.org/10.1016/0016-7037\(84\)90317-X](https://doi.org/10.1016/0016-7037(84)90317-X).
- Giggenbach W F 1988 Geothermal solute equilibria. Derivation of Na–K–Mg–Ca geothermometers; *Geochim. Cosmochim. Acta* **52(12)** 2749–2765, [https://doi.org/10.1016/0016-7037\(88\)90143-3](https://doi.org/10.1016/0016-7037(88)90143-3).
- Goswami S, Rai A K and Tripathy S 2022 Re-visiting geothermal fluid circulation, reservoir depth and temperature of geothermal springs of India; *J. Hydrol.* **612** 128131, <https://doi.org/10.1016/j.jhydrol.2022.128131>.
- GSI (Geological Survey of India) 1987 A collection of geothermal papers; *Rec. Geol. Surv. India* **115(6)** 1–206.
- GSI (Geological Survey of India) 1989 Geothermal Atlas of India; *Geol. Surv. India Spec. Publ.* **19** 143.
- GSI (Geological Survey of India) 1991 Geothermal Atlas of India; *Geol. Surv. India Spec. Publ.* **19** 10–21.
- GSI (Geological Survey of India) 1998 Geological map of India, 1:2 million scale, 7th edition.
- GSI (Geological Survey of India) 2016 Final report on monitoring discharge, temperature of hot springs in Bihar, West Bengal, Jharkhand and Odisha states; *Unpubl. Rep. FS: 2015–16*.
- GSI (Geological Survey of India) 2021 Report on assessment of geothermal energy resource potential of hot springs in and around Rajgir–Tapovan and Munger areas, Bihar; *Unpubl. Rep. FS: 2020–21*.
- Guha S K 1970 Some aspects of studies on the thermal spring of Rajgir area, Bihar. Records of papers on Ground Water Potential in Hard Rock Area; *Geol. Soc. India*.
- Gupta M L and Sukhija B S 1974 Preliminary studies of some geothermal areas in India; *Geothermics* **3(3)** 105–112, [https://doi.org/10.1016/0375-6505\(74\)90004-2](https://doi.org/10.1016/0375-6505(74)90004-2).

- Gupta B K, Prakash P and Ahmad F 2017 Water Quality of Rajgir Hot-spring, Nalanda Bihar; *Int. J. Emerg. Trends Sci. Technol.* **4(8)** 5447–5464.
- Hem J D 1985 Study and interpretation of the chemical characteristics of natural water (3rd ed); *US Geol. Surv. Water Supply Paper* **2254** 117–120.
- Hounslow A W 1995 *Water quality data: Analysis and interpretation* (1st edn); CRC Press, <https://doi.org/10.1201/9780203734117>.
- Kresic N 2010 Types and classifications of springs; In: *Groundwater hydrology of springs*, Butterworth-Heinemann, pp. 31–85.
- Krishnaswamy V S and Shankar R 1982 Scope of development, exploration and preliminary assessment of geothermal resource potentials of India; *Rec. Geol. Surv. India* **111(2)** 17–38.
- Mahon W A J, McDowell G D and Finlayson J B 1980 Carbon dioxide: Its role in geothermal systems; *NZJ Sci.* **23** 133–148.
- Mariner R H, Brook C A, Reed M J, Bliss J D, Rapport A L and Lieb R J 1983 Low-temperature geothermal resources in the western United States; In: *Assessment of low-temperature geothermal resources of the United States – 1982*; Geological Survey Circular 892, U.S. Department of the Interior, pp. 31–50.
- Mazumdar S K 1988 Crustal evolution of the Chhotanagpur gneissic complex and the mica belt of Bihar; In: *Precambrian of the Eastern Indian shield*, *Geol. Survey India Memoir* **8** 49–83.
- Mehra R N and Chowdhary S N 1966 Excavation at Devnimori: (A report of the excavation conducted from 1960 to 1963); Maharaja Sayajirao University Archaeology Series.
- Muffler L J P and White D E 1968 Origin of CO₂ in Salton Sea geothermal system, south-eastern California, USA; *Int. Geo. Congress* **17** 185–194.
- Mukherjee A and Fryar A E 2008 Deeper groundwater chemistry and geochemical modelling of the arsenic affected western Bengal basin, West Bengal, India; *Appl. Geochem.* **23** 863–894, <https://doi.org/10.1016/j.apgeochem.2007.07.011>.
- Nehring N L and D'Amore F 1984 Gas chemistry and thermometry of the Cerro Prieto, Mexico, geothermal field; *Geothermics* **13(1–2)** 75–89, [https://doi.org/10.1016/0375-6505\(84\)90008-7](https://doi.org/10.1016/0375-6505(84)90008-7).
- Nicholson K 1993 *Geothermal fluids chemistry and exploration techniques*; Springer-Verlag Berlin Heidelberg.
- Pandey G C 1975 Geochemical study of hot springs: Sitakund; *Proc. Nat. Acad. Sci. India* **45** 33–35.
- Pandey G C and Raymahashay B C 1981 Studies on some low-temperature East Indian hot springs; *Chem. Geol.* **34** 113–129, [https://doi.org/10.1016/0009-2541\(81\)90076-0](https://doi.org/10.1016/0009-2541(81)90076-0).
- Pandey G C, Pillai N V and Sharma T 1970 ¹⁸O/¹⁶O determination in thermal springs of Rajgir (Bihar); *Proc. Appl. Geochem. Earth Sci., Patna*.
- Panichi C and Gonfiantini R 1978 Environmental isotopes in geothermal studies; *Geothermics* **6** 143–161, [https://doi.org/10.1016/0375-6505\(77\)90024-4](https://doi.org/10.1016/0375-6505(77)90024-4).
- Parkhurst D L and Appelo C A J 1999 User's guide to PHREEQC (Version 2): A computer program for speciation, batch-reaction, one-dimensional transport, and inverse geochemical calculations; *Water-Resources Investigations Report* **99(4259)** 312.
- Powell T and Cumming W 2010 Spreadsheets for geothermal water and gas geochemistry; *Thirty-Fifth Workshop on Geothermal Reservoir Engineering SGP-TR-188* 1–3.
- Rai S S and Dayal R 1971 Geology and geohydrology of the South Monghyr Region, Bhagalpur Division, Bihar; *J. Soil Water Conserv.* **19(4)** 83–102.
- Raymahashay B C 1988 *Geochemistry for hydrologists*; Allied Publishers Limited.
- Razdan P N, Agarwal R K and Singh R 2008 Geothermal energy resources and its potential in India; *Earth Sci. India* **1(1)** 30–42.
- Roy R K, Chattopadhyay G S and Bisaria B K 1987 A geoscientific appraisal of Munger District, Bihar for rural development; *Geol. Surv. India Bull. Ser.* **B49**.
- Sarkar A N and Basu Mallick S 1982 Study of palaeodynamics in the Rajgir metasedimentary belt, Bihar: Stress system crustal shortening and deformation patterns; *Rec. Geol. Surv. India* **112(3)** 25–32.
- Sarkar S N, Polkanov A A, Gerling E K and Chukrov F V 1964 Geochronology of the Precambrian of peninsular India: A synopsis; *Sci. Cult.* **30** 534.
- Sarolkar P B 2018 Geothermal energy in India: Poised for development; In: *Proc. 43rd Workshop on Geothermal Reservoir Engineering*.
- Schoeller H 1977 Geochemistry of groundwater; In: *Groundwater studies – An international guide for research and practice*, UNESCO, Paris.
- Shah M, Sircar A, Shah V and Dholakia Y 2021 Geochemical and geothermometry study on hot-water springs for understanding prospectivity of low enthalpy reservoirs of Dholera Geothermal field, Gujarat, India; *Solid Earth Sci.* **6(3)** 297–312, <https://doi.org/10.1016/j.sesci.2021.04.004>.
- Shanker R 1991 Thermal and crustal structure of 'SONATA'. A zone of mid-continental rifting in Indian shield; *J. Geol. Soc. India* **37** 211–220.
- Sharma T, Pillai N V and Pandey G C 1970 ¹⁸O/¹⁶O determination in thermal springs of Rajgir, Bihar. Symposium on Applications of Geochemistry in Earth Sciences, Patna, Abstr. 36.
- Shestakova A, Guseva N, Kopylova Y, Khvaschevskaya A, Poly A and Tokarev I 2018 Geothermometry and isotope geochemistry of CO₂-rich thermal waters in Choygan, East Tuva, Russia; *Water* **10(6)** 729, <https://doi.org/10.3390/w10060729>.
- Shukla G S 1981 Geochemical interpretation of water quality in the Rajgir–Monghyr hot spring belt, India, unpublished Ph.D. thesis, IIT, Kanpur.
- Singh H K 2020 Geothermal energy potential of Indian oilfields; *Geomech. Geophys. Geo-Energy Geo-Resour.* **6(1)** 1–9.
- Singh H K, Chandrasekharam D, Vaselli O *et al.* 2015a Physico-chemical characteristics of Jharkhand and West Bengal thermal springs along SONATA mega lineament, India; *J. Earth Syst. Sci.* **124** 419–430, <https://doi.org/10.1007/s12040-015-0550-4>.
- Singh H K, Chandrasekharam D, Trupti G and Singh B 2015b Geochemistry of Rajgir–Munger Metasedimentary Springs

- of Bihar, India; *Proc. World Geotherm. Cong. Melbourne, Australia*.
- Singh H K, Sinha S K, AyazAlam M and Chandrasekharam D 2020 Tracing the evolution of thermal springs in the Hazaribagh area of Eastern Peninsular India through hydro-geochemical and isotopic analyses; *Geothermics* **85** 101817, <https://doi.org/10.1016/j.geothermics.2020.101817>.
- Stiff H A 1951 The interpretation of chemical water analysis by means of patterns; *J. Pet. Technol.* **3(10)** 15–16, <https://doi.org/10.2118/951376-G>.
- Tole M P, Ármannsson H, Zhong-He P and Árnorsson S 1993 Fluid/mineral equilibrium calculations for geothermal fluids and chemical geothermometry; *Geothermics* **22(1)** 17–37, [https://doi.org/10.1016/0375-6505\(93\)90018-I](https://doi.org/10.1016/0375-6505(93)90018-I).
- Truesdell A H and Fournier R O 1977 Procedure for estimating the temperature of a hot water component in mixed water using a plot of dissolved silica versus enthalpy; *J. Res. US Geol. Surv.* **5(1)** 49–52.
- Valdiya K S 2015 *The making of India: Geodynamic evolution*; Springer.

Corresponding editor: GEORGE MATHEW